NAS 1.60:1232

NASA TECHNICAL PAPER 1232... ANALYSIS OF PREFLUTTER AND POSTFLUTTER CHARACTERISTICS WITH MOTION-MATCHED AERODYNAMIC FORCES... SCIENTIFIC AND TECHNICAL INFORMATION OFFICE,NASA... JULY 1978

1 OF 1
24X
SUPTDOCS
GPO

AUG 14 1978

Solar 730-H-15

NAS1.60:1232

NASA Technical Paper 1232

COMPLETED
ORIGINAL

Analysis of Preflutter and Postflutter Characteristics With Motion-Matched Aerodynamic Forces

Herbert J. Cunningham

JULY 1978

NASA

33

ceter-830-H-15 NAS1.60:1232

NASA Technical Paper 1232

Analysis of Preflutter and Postflutter Characteristics With Motion-Matched Aerodynamic Forces

Herbert J. Cunningham
Langley Research Center
Hampton, Virginia

National Aeronautics
and Space Administration

**Scientific and Technical
Information Office**

1978

SUMMARY

The development of the equations of dynamic equilibrium for a lifting surface from Lagrange's equation is reviewed and restated for general exponential growing and decaying oscillatory motion. Aerodynamic forces for this motion are obtained from the three-dimensional supersonic kernel function that is newly generalized to complex reduced frequencies. An existing computer program for the kernel-function method was modified to solve the equations. Illustrative calculations were made for two flutter models at supersonic Mach numbers. Preflutter and postflutter motion isodecrement curves were obtained. Variations of motion decrement with Mach number and with air density were much milder than those predicted from conventional curves of velocity plotted against damping required (the V-g type) using simple harmonic aerodynamics. This type of analysis can be used to predict preflutter behavior during flutter testing and to predict postflutter behavior for use in the design of flutter suppression systems.

INTRODUCTION

The phenomenon analyzed here is the preflutter (decaying or subcritical) and postflutter (growing) oscillations of an aerodynamic surface in an airstream, which is a nonconservative system. For the usually analyzed condition of neutrally stable flutter motion, the equations of motion express a condition of zero net exchange of energy between the fluttering aerodynamic surface and the passing airstream. In contrast, for growing and decaying motion, a net continuing exchange of energy occurs. The approach using Lagrange's equation is reviewed and applied for this motion so as to show the way the associated aerodynamic and structural damping forces are accommodated. This approach is done in accord with the original application in reference 1 and with the reassurance given by reference 2.

Hassig in reference 3 described what is called a true-damping solution for growing or decaying motion and presented sample results obtained by using aerodynamic forces for simple harmonic motion. Those results were obtained by three solutions called the p-method, the p-k method, and the k-method. Each of these solution methods gives near flutter results that are approximate because of the simple harmonic aerodynamics employed. Of the three, the p-k method is believed to give the nearest approximation to what would be obtained with the motion-matched aerodynamic forces, as developed and used in the present paper.

A few analyses of near-flutter motion with motion-matched aerodynamic forces have been reported. Dugundji, Dowell, and Perkin include in references 4 and 5 analyses and results for the unstable motion of panels at speeds greater than the flutter speed by permitting a complex wave speed for the traveling waves of panel deflection. Morino presents in reference 6 the development of an aerodynamic potential by using a Green's function for timewise arbitrary motions. Some applications of this method given in reference 7 show generalized

aerodynamic coefficients for growing, steady, and decaying oscillations of a rectangular wing at supersonic speeds and some chordwise distributions of pressure coefficient for growing oscillations of a wing-body-tail configuration pitching in a subsonic flow. As part of its overall development based on the Laplace transform technique, reference 8 gives certain functions for general exponential motions in two-dimensional flow. These are the generalized Theodorsen circulation function for two-dimensional incompressible flow and the velocity potential and associated lift and moment functions for two-dimensional supersonic flow.

In the present paper the aerodynamic forces for the growing and decaying oscillatory motion are obtained by generalizing to complex frequency the supersonic three-dimensional velocity potential of reference 9 and the kernel function of reference 10. The analysis is illustrated by applying at supersonic speeds to two flutter-tested configurations the kernel-function aerodynamic forces in a computer program modified from that of reference 11. This type of analysis has applications to the prediction of motion decrements during wind-tunnel and flight flutter testing and to the design of automatic controls for flutter suppression.

The appendix reviews the relation between the structural damping coefficient and the logarithmic decrement of motion in the presence of solid-friction structural damping (mechanical hysteresis) as used in the analysis.

SYMBOLS

a	real part of p (see eq. (2))
b_m	half of mean geometric chord
b_0	half of root chord (see fig. 1)
c	speed of sound
g	structural damping coefficient
h	shape of modal deflection (see eq. (4))
i	unit of imaginaries, $\sqrt{-1}$
K	supersonic kernel function
k	reduced frequency, $\omega b_0/V$
l	reference length
M	Mach number
m	mass per unit area
m_i	generalized mass of mode i (see eqs. (20))

p	exponential coefficient of motion in e^{pt}
Δp	lifting pressure, positive with z
Q_i	generalized force (see eq. (5))
Q_{ij}	element of generalized aerodynamic-force matrix (see eq. (14))
q	generalized coordinate of motion
$\bar{q}$	amplitude of q (see eq. (4))
S	area of lifting surface
s	ratio of semispan to root chord (see fig. 1)
T	kinetic energy of structure
t	time
U	potential energy of structure
$U(\ )$	unit function (see eq. (29))
V	free-stream speed
w	downwash on lifting surface
$\bar{w}, W$	time and space varying functions, respectively, in w (see eq. (24))
x, y, z	right-hand Cartesian coordinates, x positive to rear, z positive upward
x_0	$= x - \xi$
y_0	$= y - \eta$
z	z-coordinate of deflection shape
β	$= \sqrt{M^2 - 1}$
δ	logarithmic decrement of motion (see eqs. (3), (A3), and (A7))
$\delta q, \delta W$	virtual displacement and virtual work, respectively
η_1, η_2	limits of η-integration (see eq. (25))
θ	$= 1 - i\frac{a}{\omega}$ (see eq. (2))
μ	mass ratio

ξ, η dummy variable for x and y, respectively, representing locations of sources and doublets

ρ air density

σ effective spring stiffness of structure (see eq. (7))

τ variable of integration in K

τ_u, τ_l limits of integration in K

τ_1, τ_2 times of origination of disturbances that affect point (x,y) at time t (see eq. (25))

ϕ_u perturbation velocity potential on upper surface

ψ_D potential function for doublet located at origin

Ω_δ $= \left(\frac{\omega_b}{\omega}\right)^2 \left(1 - i \frac{\delta}{\pi}\right)$ (see eq. (22))

ω circular frequency of motion

$\bar{\omega}$ $= \omega / V\beta^2$

ω_b base or reference frequency

ω_i, ω_j natural frequencies of modes i and j, respectively

Subscripts:

aero contribution from aerodynamic forces

b base or reference mode

i,j modes

sf solid friction (mechanical hysteresis)

Mathematical notation:

$(\dot{})$ first time derivative, $\partial( )/\partial t$

$(\ddot{})$ second time derivative, $\partial^2( )/\partial t^2$

ANALYSIS

General Exponential Motion

For the purpose of this paper it is sufficient to analyze the perturbations of an initially plane surface. Figure 1 shows the lifting surface and the coordinate system. Essentially all findings apply to nonplanar and multiple lifting surfaces as well, but the procedure is illustrated without the complications of nonplanar and multiple surfaces. The surface analyzed has its timewise mean location in the plane $z = 0$. The z-coordinate of the instantaneous perturbation away from the mean location of the surface is

$$z(x,y,t) = Z(x,y)e^{pt} \tag{1}$$

where the space variation $Z(x,y)$ can be complex. The exponential coefficient p is of the form

$$p \equiv a + i\omega = i\omega\left(1 - i\,\frac{a}{\omega}\right) = i\omega\theta \tag{2}$$

where $i = \sqrt{-1}$ is the unit of imaginaries, ω is the circular frequency, and a is the exponential time rate of growth of motion. For $a/\omega \ll 1$

$$p = i\omega\left(1 + i\,\frac{\delta}{2\pi} + O(\delta^2)\right) \sim i\omega\left(1 + i\,\frac{\delta}{2\pi}\right) \tag{3}$$

where δ is the logarithm of the ratio of the amplitudes at the beginning and end of one complete cycle and is positive for a decaying oscillation. It is commonly called the log decrement. (See appendix.)

Equations of Equilibrium

For the general unsteady aerodynamic forces considered here, direct solution of the equations of motion for flutter is usually not feasible. Accordingly the flutter deflection is approximated in the usual way by a finite modal series

$$z(x,y,t) \sim \sum_i q_i(t)\, h_i(x,y) \tag{4}$$

$$q_i(t) = \bar{q}_i e^{pt}$$

where the modal deflections $h_i(x,y)$ are real functions as specified in reference 2, and $\bar{q}_i$ is the complex amplitude of $q_i(t)$.

The equilibrium equations are obtained from Lagrange's equation, which is a specialized form of the principle of virtual work

$$\frac{d}{dt}\left(\frac{\partial T}{\partial \dot{q}_i}\right) - \frac{\partial T}{\partial q_i} + \frac{\partial U}{\partial q_i} = Q_i \qquad (i = 1, 2, \ldots) \tag{5}$$

where T is the kinetic energy, U is the potential energy (elastic only in the present use), and Q_i is the generalized force associated with the generalized displacement q_i and is obtained from the virtual work due to external forces (aerodynamic forces and structural damping).

The kinetic energy of the structure is

$$T = \int_S \frac{1}{2}\, m(x,y)\left(\sum_i \dot{q}_i\, h_i(x,y)\right)^2 dS \tag{6}$$

where S is the area of the lifting surface, and $m(x,y)$ is its mass per unit area. The elastic potential energy is represented by

$$U = \int_S \frac{1}{2}\, \sigma(x,y)\left(\sum_i q_i\, h_i(x,y)\right)^2 dS \tag{7}$$

where $\sigma(x,y)$ represents the effective spring stiffness rate of the elastic restoring force.

Application of Lagrange's equation in the absence of external forces gives

$$\sum_j \ddot{q}_j \int_S m(x,y)\, h_i(x,y)\, h_j(x,y)\, dS + \sum_j q_j \int_S \sigma(x,y)\, h_i(x,y)\, h_j(x,y)\, dS = 0 \tag{8}$$

Using the relationships (see eq. (4))

$$\left.\begin{aligned} q_j &\equiv q_j(t) = \bar{q}_j e^{pt} \\ \dot{q}_j &\equiv \dot{q}_j(t) = p\bar{q}_j e^{pt} = pq_j \\ \ddot{q}_j &\equiv \ddot{q}_j(t) = p^2\bar{q}_j\, e^{pt} = p^2 q_j = -(\omega\theta)^2 q_j \end{aligned}\right\} \tag{9}$$

in equation (8) gives

$$\sum_j q_j \int_S \sigma h_i h_j \, dS = \sum_j (\omega_j \theta)^2 q_j \int_S m h_i h_j \, dS \tag{10}$$

which is the usual Rayleigh type approximation for replacing the elastic restoring forces involving σ in terms of the mass-inertia terms involving $m\omega_j{}^2\theta^2$. Note that in the absence of external forces, $a = 0$, $p = i\omega$, and ω becomes the modal eigenvalue ω_j.

The virtual work is that done by the external forces moving through the virtual displacement $h_i \delta q_i$; thus,

$$\delta W = \delta W_{aero,i} + \delta W_{sf,i}$$

The aerodynamic contribution is expressed initially by

$$\delta W_{aero,i} = \int_S \Delta p(x,y,t) \; h_i(x,y) \; \delta q_i(t) \, dS \tag{11}$$

The lifting pressure distribution Δp is approximated by a modal series parallel to that for deflection z in equation (4); thus,

$$\Delta p(x,y,t) = \sum_j \frac{1}{l} q_j(t) \; \Delta p_j(x,y) \tag{12}$$

where l is a user-selected reference length such as $2b_0$, and Δp_j is the complex amplitude of the lifting pressure distribution caused by and associated with the modal deflection $h_j(x,y)$. With substitutions of the series of equations (4) and (12)

$$\delta W_{aero,i} = \int_S \left(\sum_j \frac{q_j}{l} \Delta p_j \right) (h_i \delta q_i) \, dS$$

$$= Q_{aero,i} \delta q_i \qquad (i = 1, 2, \ldots) \tag{13}$$

from which is obtained

$$Q_{aero,i} = \int_S \sum_j \frac{q_j}{l} \Delta p_j h_i \, dS$$

$$= \sum_j q_j Q_{ij} \tag{14}$$

where the generalized aerodynamic-force element

$$Q_{ij} \equiv \int_S \frac{1}{2} \Delta p_j h_i \, dS \tag{15}$$

This development is valid for real mode shapes h_i as determined in reference 2 and as discussed in C,17 of reference 12.

The solid-friction structural damping force is of the same form as in the damping term of equation (A5) of the appendix. Thus,

$$\delta W_{sf,i} = \int_S \sigma(x,y) \frac{\gamma}{\omega} \sum_j h_j \dot{q}_j (-g_{sf,j}) h_i \delta q_i \, dS \tag{16}$$

Use of equation (4) gives

$$\delta W_{sf,i} = \int_S \left(-i\sigma \sum_j q_j h_j g_{sf,j} \right) h_i \delta q_i \, dS$$

$$= Q_{sf,i} \delta q_i \tag{17}$$

where the structural damping coefficient $g_{sf,j}$ can differ among the modes j. The contribution to Q_i is

$$Q_{sf,i} = -i \sum_j g_{sf,j} q_j \int_S \sigma h_i h_j \, dS \tag{18}$$

Using the equality developed in equation (10)

$$Q_{sf,i} = -i \sum_j g_{sf,j} (\omega_j \theta)^2 q_j \int_S m h_i h_j \, dS \tag{19}$$

The equality given by equation (10) applied for the condition of no external forces, and the modes and frequencies are thus for the natural undamped or normal modes for which h_i and h_j are orthogonal with respect to the mass distribution; that is,

$$m_i = \int_S m h_i h_j \, dS$$

$$m_i = \begin{cases} \int_S m h_i^2 \, dS & (j = i) \\ 0 & (j \neq i) \end{cases} \qquad (20)$$

Substitution of these developments into Lagrange's equation (5) gives

$$-\omega^2 \theta^2 m_i q_i + \omega_i^2 (1 + i g_i) m_i q_i - \sum_j q_j Q_{ij} = 0 \qquad (i = 1, 2, \ldots) \qquad (21)$$

In order to put the equilibrium equations into a form for routine solution by a complex eigenvalue subroutine divide by

$$-\omega^2 \theta^2 (1 + i g_i) (\omega_i / \omega_b)^2 m_i$$

Then the result is (for $\delta/\pi \ll 1$)

$$\left[-\Omega_\delta + \left(\frac{\omega_b}{\omega_i} \right)^2 (1 + i g_i)^{-1} \right] q_i + \frac{(\omega_b/\omega_i)^2}{m_i (1 + i g_i) \omega^2 \left(1 + i \frac{\delta}{\pi} \right)} \sum_j \frac{q_j}{l} \int_S \Delta p_j h_i \, dS = 0$$

$$(i = 1, 2, \ldots) \qquad (22)$$

where

$$\Omega_\delta \equiv \left(\frac{\omega_b}{\omega} \right)^2 \left(1 - i \frac{\delta}{\pi} \right)$$

A matched solution is obtained when the output value of the log decrement from an eigenvalue Ω_δ matches the preselected input value in Δp_j and in the denominator term $1 + i\delta/\pi$. (The lifting pressure Δp_j is a function of δ as well as of x, y, M, and k.) For the case of simple harmonic aerodynamics (input $\delta = 0$), equation (22) reverts to the conventional flutter equation, and $-\delta/\pi$ in the eigenvalue is equivalent to and interpretable as the conventionally used structural damping coefficient g.

Aerodynamic Forces for General Exponential Motion

The lifting pressure distribution for general exponential motion required in equations (15) and (22) can be obtained for supersonic speeds by generalization to complex frequencies of the results of references 9 and 10.

Velocity potential in supersonic flow.- The velocity potential analysis of reference 9 is applied here to the general case of exponentially growing and decaying oscillatory motion; that is, with the time variation of downwash

$$\bar{w}(t) = e^{i\omega t} e^{at} = e^{(a+i\omega)t} = e^{i\omega\theta t} \tag{23}$$

where a and ω are real, and

$$\theta \equiv 1 - i\frac{a}{\omega}$$

Where a lifting surface is analyzed as a distribution of source-sink pairs over the projection of the lifting surface onto the plane $z = 0$ (see fig. 1), the local strength of the source-sink pairs is proportional to the local downwash

$$w(x,y,z=0,t) = W(x,y)\,\bar{w}(t) \tag{24}$$

(The notation here is mostly parallel to that of ref. 9.) Parallel to equation (15) of reference 9, the velocity potential for the upper surface is (in the plane $z = 0$)

$$\phi_u(x,y,t) = \int_0^x \int_{\eta_1}^{\eta_2} \frac{W(\xi,\eta)}{-2\pi\beta} \frac{\bar{w}(t-\tau_1) + \bar{w}(t-\tau_2)}{\sqrt{(\eta-\eta_1)(\eta_2-\eta)2b_0}}\, d(2b_0\eta)\, d(2b_0\xi) \tag{25}$$

where

$$\eta_1 = y - \frac{x-\xi}{\beta}$$

$$\eta_2 = y + \frac{x-\xi}{\beta}$$

$$\tau_1 = \frac{M(x-\xi)2b_0}{c\beta^2} - \frac{\sqrt{(\eta-\eta_1)(\eta_2-\eta)}}{c\beta}\,2b_0$$

$$\tau_2 = \frac{M(x-\xi)2b_0}{c\beta^2} + \frac{\sqrt{(\eta-\eta_1)(\eta_2-\eta)}}{c\beta}\,2b_0$$

$$\beta \equiv \sqrt{M^2 - 1}$$

c is the speed of sound, and ξ and η are dummy variables for x and y, respectively. The velocity potential for the lower surface is the negative of that for the upper surface. In the integrand the time variation is

$$\bar{w}(t - \tau_1) + \bar{w}(t - \tau_2) = e^{a(t-\tau_1)} e^{i\omega(t-\tau_1)} + e^{a(t-\tau_2)} e^{i\omega(t-\tau_2)}$$

$$= e^{(a+i\omega)t} e^{-(a+i\omega)(\tau_2+\tau_1)/2} \left[e^{(a+i\omega)(\tau_2-\tau_1)/2} + e^{-(a+i\omega)(\tau_2-\tau_1)/2} \right]$$

$$= e^{i\omega\theta t} e^{-i\omega\theta(\tau_2+\tau_1)/2} \; 2 \cos\left(\omega\theta \frac{\tau_2 - \tau_1}{2}\right)$$

$$= e^{i\omega\theta t} e^{-i\omega\theta M x_0 2b_0/c\beta^2} \; 2 \cos\left(\omega\theta \frac{\sqrt{x_0^2 - \beta^2 y_0^2}\, 2b_0}{c\beta^2}\right) \qquad (26)$$

This time variation is the same as that just before equation (19) of reference 9, except that ω is replaced by $\omega\theta$. Thus, for the upper surface

$$\phi_u(x,y,t) = \frac{-e^{i\omega\theta t}}{\pi} \int_0^x \int_{\eta_1}^{\eta_2} W(\xi,\eta)\, U(x_0 - \beta|y_0|) e^{-i\omega\theta M 2b_0 x_0/c\beta^2}$$

$$\times \cos\left(\frac{\omega\theta 2b_0\sqrt{x_0^2 - \beta^2 y_0^2}}{c\beta^2}\right) \frac{d(2b_0\eta)\; d(2b_0\xi)}{2b_0\sqrt{x_0^2 - \beta^2 y_0^2}} \qquad (27)$$

where

$$x_0 \equiv x - \xi$$

$$y_0 \equiv y - \eta$$

Acceleration potential and kernel function in supersonic flow.- As shown in the preceding section for an exponentially growing (or decaying) oscillatory

motion with time variation $e^{i\omega\theta t}$, the velocity potential is the same as that for a simple harmonic motion $e^{i\omega t}$, with ω replaced by $\omega\theta$.

Given the relationship between velocity potential, acceleration potential, and the kernel function shown in equations (8) to (12) of reference 10, the same replacement of $\omega\theta$ for ω, $k\theta$ for k, and $\omega\theta$ for ω applies throughout. This is true for supersonic flow because the integrations back over events originating in past time, extend over only a finite time, and are therefore distinct and finite.

Thus the potential for the doublet located at the origin is

$$\psi_D = 2\frac{\partial}{\partial(2b_0 z)}\frac{e^{i\omega\theta t}e^{-iM^2\bar{\omega}\theta 2b_0 x}\cos\left(M\bar{\omega}\theta 2b_0\sqrt{x^2-\beta^2(y^2+z^2)}\right)}{2b_0\sqrt{x^2-\beta^2(y^2+z^2)}} \tag{28}$$

where $\bar{\omega} \equiv \omega/V\beta^2$. Equation (28) is a generalization of equation (4) of reference 10. The planar ($z = 0$) supersonic kernel can be used in the form

$$K(x_0,y_0) = \frac{-2}{V(2b_0)^2 y_0^2}e^{-ik\theta x}\,U(x_0-\beta|y_0|)\left[\frac{x_0 e^{-ik\theta x_0/\beta^2}}{\sqrt{x_0^2-\beta^2y_0^2}}\cos\left(\frac{Mk\theta}{\beta^2}\sqrt{x_0^2-\beta^2y_0^2}\right)\right.$$

$$\left. + \frac{ik\theta|y_0|}{2}\int_{\tau_l}^{\tau_u}\frac{\tau}{\sqrt{1+\tau^2}}e^{-ik\theta|y_0|\tau}\right]d\tau \tag{29}$$

where the unit function

$$U(x_0-\beta|y_0|) = \begin{cases}1 & (x_0-\beta\,y_0 > 0)\\ 0 & (x_0-\beta\,y_0 \le 0)\end{cases}$$

and

$$\tau_l = \frac{1}{\beta^2|y_0|}\left(x_0 - M\sqrt{x_0^2-\beta^2y_0^2}\right)$$

$$\tau_u = \frac{1}{\beta^2|y_0|}\left(x_0 + M\sqrt{x_0^2-\beta^2y_0^2}\right)$$

Equation (29) is a generalization of equation (16c) of reference 10. A similar generalization applies to the nonplanar kernel for supersonic flow such as that presented in reference 13 (with sign corrections as explained in section entitled "Results and Discussion").

Method of Solution of Equations

Numerical solutions of the equilibrium equations are made for a model with known parameters by first selecting values of M, k, and δ and then solving the set of equations (29) for its eigenvalues Ω_δ for each of a selected range of values of air density ρ, usually beginning with $\rho = 0$. From each eigenvalue a frequency ω and output value of decrement δ are extracted, and associated parameters, such as flutter-speed index or stiffness-altitude parameter, can be calculated as desired. Plots of desired results are made for the range of ρ used, with attention given to properly connecting the modal roots. Particular attention is given to finding the values of ρ for which the output δ equals the input δ. These values indicate matched conditions. (The important matched points are usually those near the flutter crossing with the lowest dynamic pressure, called the critical crossing.) For a particular k-value the matched-point results may not fall in the desired range of density or mass ratio. In this case a new k-value can usually be estimated on the basis of a constant dynamic pressure and constant frequency. This estimate gives k proportional to $\sqrt{\rho}$, which is also proportional to $\sqrt{1/\mu}$.

RESULTS AND DISCUSSION

Analytical results have been obtained by using a modified version of the computer program in reference 11. This program employs supersonic kernel-function aerodynamics. For calculating supersonic kernel-function values for complex reduced frequencies, it was convenient to use subroutines based on the appendix of reference 13. (In ref. 13 the series summations with the coefficients a_m and b_m have incorrect signs that were reversed in the present use.) Downwash collocation values and modal deflections for calculating generalized aerodynamic forces were obtained by interpolating the experimental modal deflection data by using a surface-spline computer program based on the analysis in reference 14. Certain experimental modal deflection data had sufficient irregularity to require smoothing, especially in obtaining streamwise slopes for downwash collocation. Accordingly the spline program was modified so that, in effect, the modal data were attached to the spline by a uniform set of rather stiff springs.

Clipped-Tip Delta-Wing Model

Experimental mode-shape, natural-frequency, and mass data for a clipped-tip delta-wing model are given in tables I to III of reference 15. The first six natural modes were used in the present calculations. (Spot checks for modal convergence with nine modes indicate that six modes are sufficient for convergence.)

Simple harmonic aerodynamics.- For $M = 1.3$, $k = 0.47$, $g_i = 0$, and $\delta = 0$ (simple harmonic aerodynamics), figures 2(a) and 2(b) display two associated results, $-\delta/\pi$ plotted against flutter-speed index $V/b_m\omega_2\sqrt{\mu}$ and against ρ, respectively. Figure 2(a) includes a sketch of the wing-model planform. Only the mode 2 traces are plotted because this mode gives the critical flutter crossing (lowest $V/b_m\omega_2\sqrt{\mu}$). In the flutter-speed index b_m and μ are as in ref-

erence 15; b_m is one-half the mean geometric chord, and μ is the ratio of the wing mass to the mass of air contained in the frustum of a cone that just encloses the wing.

The crossing points at $\delta/\pi = 0$ are the ones that match the input $\delta = 0$ in the aerodynamic forces for simple harmonic motion and give the values of $V/b_m\omega_2\sqrt{\mu}$ and ρ at the flutter boundary for this M, k, and other parameters. At the end of the section entitled "Analysis" it was pointed out that, for input $\delta = 0$, $-\delta/\pi$ is interpretable as the conventional g. Thus the curve in figure 2(a) is a V-g type. In some past analyses V-g curves have been interpreted as predicting rates of growth and decay of the oscillatory motion. (See, e.g., ref. 16 and the description of the k-method in ref. 3.) The two labeled points at 0.05 and -0.05 could accordingly be interpreted to indicate near-flutter motion with log decrements of motion of -0.05π and 0.05π, respectively, but such an interpretation does not match the input δ in the aerodynamic forces. In figure 2(b) the three points discussed ($\delta = 0$, $-\delta/\pi = 0.05$ and -0.05) are projected to a plot of ρ against $V/b_m\omega_2\sqrt{\mu}$. (The latter scale is at the upper right.) These three points are used in subsequent figures.

Matched aerodynamics for growing and decaying motion, $\delta \neq 0$.- Now consider the result of using input values $-\delta/\pi = \pm 0.05$. Figures 3(a) and 3(b) show the same type of results as those in figures 2(a) and 2(b). The mode 2 traces for $\delta = 0$ are replotted here. Segments of the traces for input $-\delta/\pi = \pm 0.05$ are plotted, and the matched crossing points are indicated. At the lower motion-matched point $-\delta/\pi = -0.05$, the decay rate for the predicted motion matches that of the aerodynamics. Similarly at the upper motion-matched point $-\delta/\pi = 0.05$, the growth rate for the predicted motion matches that of the aerodynamics. The three motion-matched points are projected to a plot of ρ against $V/b_m\omega_2\sqrt{\mu}$. (The latter scale is at the upper right in fig. 3(b).)

The question arises as to whether there is a significance to points on these curves that do not match the input δ. Such points can be interpreted to represent ordinate values of $-\delta/\pi + g$, where g is the uniform-for-all-modes increment of g that would make those other points the ones of matched motion. For example, in figure 3(a) on the curve segment for $-\delta/\pi = -0.05$, the point with an ordinate of -0.03 represents $(-\delta/\pi) + g = -0.03$, from which $g = 0.02$.

Thus far only one value of $k = 0.47$ has been presented. Figure 4 presents the results from solutions for a range of k-values from about 0.33 to about 0.55. The flutter-speed index $V/b_m\omega_2\sqrt{\mu}$ is plotted against density ρ. The three points from figure 2(b) obtained with simple harmonic aerodynamics ($\delta = 0$) and the three points from figure 3(b) obtained with motion-matched aerodynamics are indicated by the symbols. The point for $\delta = 0$ is common to the two sets. Solutions from a range of k give the isodecrement curves shown, solid-line curves for the three motion-matched values and dashed-line curves from a V-g type prediction that used simple harmonic aerodynamics. Curves for other decrement rates δ are not plotted.

Use of isodecrement results.- An example of the use of isodecrement curves is shown in figure 5. The isodecrement curves from figure 4 are included in figure 5. A possible wind-tunnel operating curve is shown in figure 13 of reference 15. In this reference the vertical lines to the flutter boundary are for

fixed M and increasing dynamic pressure. An example of that general type of tunnel operating curve (fixed M and c and increasing ρ) is included in figure 5 rising from the lower left. The intersections of the operating curve with the isodecrement curves give the associated values of flutter-speed index and ρ. Projections can be made as shown in figure 5 to obtain the associated plot of decrement against density. On this plot the rate of change of the decrement with increasing ρ predicted from the matched aerodynamics (the solid-line curves) is readily seen to be sharply less (about one-third) than is predicted from V-g type curves with simple harmonic aerodynamics (the dashed-line curves).

The preceding results are for M = 1.3. Similar results have been calculated over a moderate range of supersonic M and are shown in figure 6. Boundaries of flutter-speed index are plotted against M. The contrast between the two types of prediction is virtually the same throughout the Mach number range.

All-Movable Horizontal-Tail Flutter Model

Flutter model HT-7 of figures 6 and 7 of reference 17 was also analyzed. It is a semispan model of an all-movable horizontal tail. In figure 7(a) the flutter-speed index is plotted against M, and the same type of boundaries as before are shown. The density ρ is 1.70 kg/m^3, which is the density of the experiment at M = 1.64. For this case the contrast between the two types of prediction is even stronger; that is, the dashed-line curves from a V-g type prediction with simple harmonic aerodynamics (input $\delta = 0$) are very close to the flutter boundary, thereby indicating a steep gradient of motion decrement with changing M. (Although not presented here, the gradient-of-motion decrement with changing density for fixed M and c is also very steep from a V-g type prediction.) Observation of the solid-line curves from motion-matched aerodynamics shows a small rate of change of motion decrement with changing M. That rate of change is also small with changing ρ for fixed M and c.

Figure 7(b) gives the same results for model HT-7 in terms of stiffness-altitude parameter plotted against M as in reference 17. In figures 7(a) and 7(b) the upper Mach number limit of the calculated boundaries is the value of M for a sonic leading edge, which is the upper limit for the supersonic kernel-function computer program used.

CONCLUDING REMARKS

The equations of dynamic equilibrium are reviewed for a lifting surface in an airstream undergoing general exponential motion, that is, growing and decaying oscillations. With the appropriate motion-matched aerodynamics in these equations, analyses are made of preflutter (subcritical) motion and postflutter motion, as well as the usual flutter boundary.

The three-dimensional supersonic velocity potential and kernel function were generalized to complex reduced frequencies appropriate for growing and decaying oscillatory motions. An existing computer program for the kernel-function method was modified for the eigensolution of the equilibrium equations.

Illustrative calculations were made for two flutter models for which these aerodynamic forces are applicable. In addition to the usual flutter boundary for zero motion decrement, example isodecrement curves were calculated for selected decaying and growing motion decrements. For these two models the rates of change of the motion decrement as functions of Mach number and air density were found to be much milder than the rates of change predicted from V-g type (velocity plotted against damping required) curves using simple harmonic (zero decrement) aerodynamics.

This type of analysis has applications to the prediction of motion decrements during wind-tunnel and flight flutter testing and to the design of automatic controls for flutter suppression.

Langley Research Center
National Aeronautics and Space Administration
Hampton, VA 23665
May 31, 1978

APPENDIX

THE RELATION OF SOLID-FRICTION (MECHANICAL HYSTERESIS) DAMPING TO THE DAMPING DECREMENT OF EXPONENTIAL MOTION

The differential equation of motion of a simple spring-mass-damper system subjected to a continuous simple harmonic forcing function is, in complex notation

$$m\ddot{x} + c\dot{x} + kx = Fe^{i(\omega t+\alpha)} \tag{A1}$$

where x is displacement, m, c, and k are constants representing mass, damper constant, and spring constant, respectively, F is the real amplitude of the forcing function, and α is the phase angle between F and x. The solution of equation (A1) is

$$x = n\frac{F}{k}e^{i(\omega t+\alpha-\eta)} \tag{A2}$$

where the magnification factor n is a function of m, c, and k, and η is the phase delay angle.

For free oscillations (i.e., $F = 0$), the logarithmic decrement δ of the ratio of amplitudes at the beginning and end of one complete cycle is

$$\delta = 2\pi\frac{c/c_{cr}}{\sqrt{1-(c/c_{cr})^2}} = 2\pi\frac{c}{c_{cr}} + O\left[\left(\frac{c}{c_{cr}}\right)^2\right] \sim 2\pi\frac{c}{c_{cr}} \tag{A3}$$

where c_{cr} is the critical value of c.

For solid-friction structural damping (mechanical hysteresis) experimental results (see refs. 18 and 19) have shown that for forced simple harmonic motion the energy dissipated (converted to heat) by the structural damping is proportional to the motion amplitude squared but varies little with frequency. Consequently a good approximation is to make the replacement

$$c\omega = kg \tag{A4}$$

where g is the structural damping coefficient, and to treat k, g, and kg as constant. Thus for solid-friction damping

$$m\ddot{x} + \frac{kg}{\omega}\dot{x} + kx = Fe^{i(\omega t+\alpha)} \tag{A5}$$

for which

$$\ddot{x} + \omega_n^2(1 + ig)x = \omega_n^2 \frac{F}{k} e^{i(\omega t+\alpha)} \tag{A6}$$

where

$$\omega_n^2 = \frac{k}{m}$$

The solution of equation (A6) has the same form as equation (A2).

For the case of free oscillations with solid-friction damping, the method described by Bishop in reference 20 is based on the assumption that equation (A4) is still an adequate approximation for exponentially damped oscillations, even though the motion is not simple harmonic. (In actual practice the common method of experimentally determining g is to measure the decay of a free oscillation.) Thus,

$$\delta = \frac{2\pi g}{1 + \sqrt{1 - g^2}} = \pi g + O(g^2) \sim \pi g \tag{A7}$$

This result is that of reference 21 and, through the order of g, is the same as that of references 22, 23, and others.

REFERENCES

1. Loring, S. J.: General Approach to the Flutter Problem. SAE J., vol. 49, no. 2, Aug. 1941, pp. 345-355.

2. Nilsson, J. E. V.; and Langefors, N. B.: Generalized Complex Forces in Flutter Calculations. J. Aeronaut. Sci., vol. 18, no. 2, Feb. 1951, p. 139.

3. Hassig, Hermann J.: An Approximate True Damping Solution of the Flutter Equation by Determinant Iteration. J. Aircr., vol. 8, no. 11, Nov. 1971, pp. 885-889.

4. Dugundji, John; Dowell, Earl; and Perkin, Brian: Subsonic Flutter of Panels on Continuous Elastic Foundations. AIAA J., vol. 1, no. 5, May 1963, pp. 1146-1154.

5. Dowell, Earl H.: Flutter of Infinitely Long Plates and Shells. Part I: Plate. AIAA J., vol. 4, no. 8, Aug. 1966, pp. 1370-1377. Part II: Cylindrical Shell. AIAA J., vol. 4, no. 9, Sept. 1966, pp. 1510-1518.

6. Morino, Luigi: A General Theory of Unsteady Compressible Potential Aerodynamics. NASA CR-2464, 1974.

7. Tseng, Kadin; and Morino, Luigi: Fully Unsteady Subsonic and Supersonic Potential Aerodynamics of Complex Aircraft Configurations for Flutter Applications. AIAA/ASME/SAE 17th Structures, Structural Dynamics, and Materials Conference, May 5-7, 1976, pp. 626-638.

8. Edwards, John William: Unsteady Aerodynamic Modeling and Active Aeroelastic Control. SUDAAR 504 (NASA Grant NGL-05-020-007), Stanford Univ., Feb. 1977. (Available as NASA CR-148019.)

9. Garrick, I. E.; and Rubinow, S. I.: Theoretical Study of Air Forces on an Oscillating or Steady Thin Wing in a Supersonic Main Stream. NACA Rep. 872, 1947. (Supersedes NACA TN 1383.)

10. Watkins, Charles E.; and Berman, Julian H.: On the Kernel Function of the Integral Equation Relating Lift and Downwash Distributions of Oscillating Wings in Supersonic Flow. NACA Rep. 1257, 1956. (Supersedes NACA TN 3438.)

11. Cunningham, Herbert J.: Computer Program for Supersonic Kernel-Function Flutter Analysis of Thin Lifting Surfaces. NASA TM X-2913, 1974.

12. Flax, Alexander H.: Aeroelasticity and Flutter. High Speed Problems of Aircraft and Experimental Methods, A. F. Donovan, H. R. Lawrence, F. E. Goddard, and R. R. Gilruth, eds., Princeton Univ. Press, 1961, pp. 161-423.

13. Cunningham, Atlee M., Jr.: Oscillatory Supersonic Kernel Function Method for Interfering Surfaces. J. Aircr., vol. 11, no. 11, Nov. 1974, pp. 664-670.

14. Harder, Robert L.; and Desmarais, Robert N.: Interpolation Using Surface Splines. J. Aircr., vol. 9, no. 2, Feb. 1972, pp. 189-191.

15. Sandford, Maynard C.; Abel, Irving; and Gray, David L.: Development and Demonstration of a Flutter-Suppression System Using Active Controls. NASA TR R-450, 1975.

16. Richardson, J. R.: A More Realistic Method for Routine Flutter Calculations. AIAA Symposium on Structural Dynamics and Aeroelasticity, Aug.-Sept. 1965, pp. 10-17.

17. Cunningham, Herbert J.: Application of a Supersonic Kernel-Function Procedure to Flutter Analysis of Thin Lifting Surfaces. NASA TN D-6012, 1970.

18. Kimball, A. L.; and Lovell, D. E.: Internal Friction in Solids. Phys. Rev., vol. 30, no. 6, Dec. 1927, pp. 948-959.

19. Becker, E.; and Föppl, O.: Dauerversuche zur Bestimmung der Festigkeitseigenschaften, Beziehungen zwischen Baustoffdämpfung und Verformungs geschwindigkeit. Forschungsarb. Geb. Ingenieurwes., Heft 304, 1928.

20. Bishop, R. E. D.: The Treatment of Damping Forces in Vibration Theory. J. R. Aeronaut. Soc., vol. 59, no. 539, Nov. 1955, pp. 738-742.

21. Neumark, S.: Concept of Complex Stiffness Applied to Problems of Oscillations With Viscous and Hysteretic Damping. R. & M. No. 3269, British A.R.C., 1962.

22. Myklestad, N. O.: Vibration Analysis. McGraw-Hill Book Co., Inc., 1944.

23. Scanlan, Robert H.; and Rosenbaum, Robert: Introduction to the Study of Aircraft Vibration and Flutter. Macmillan Co., c.1951; Dover Publications, Inc., c.1968.

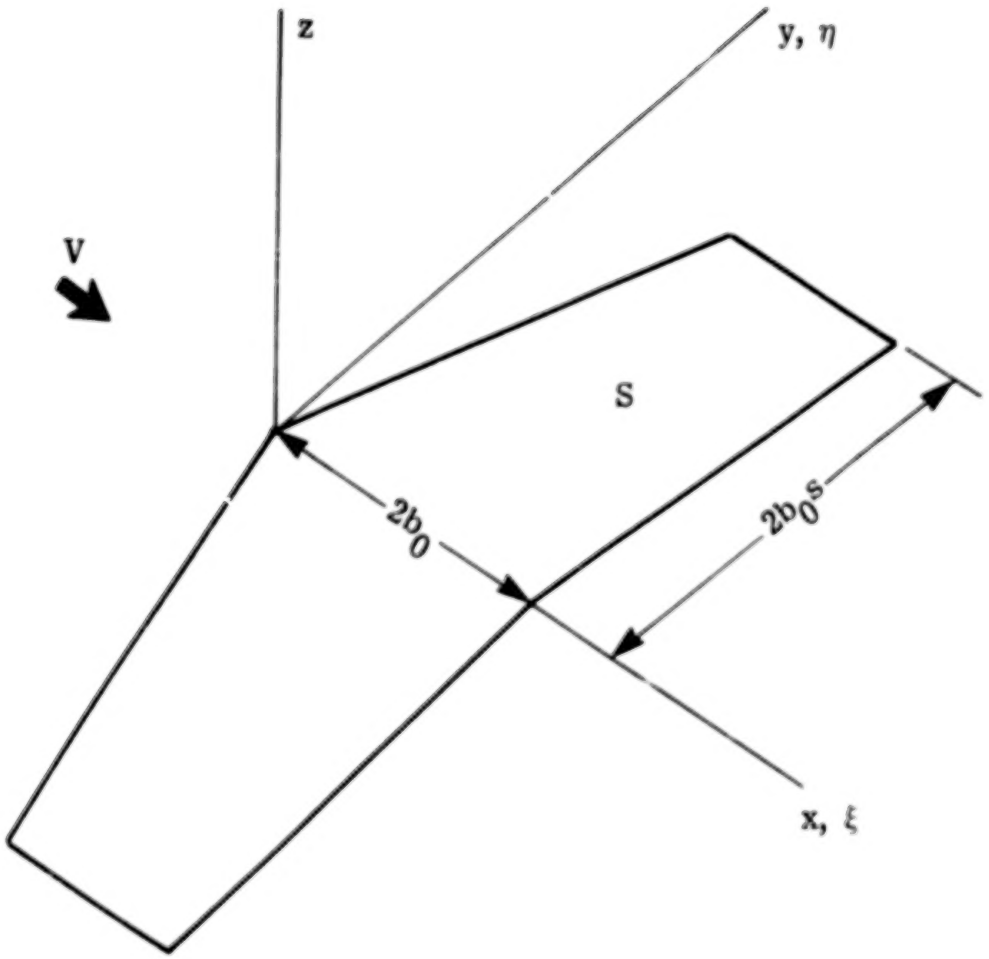
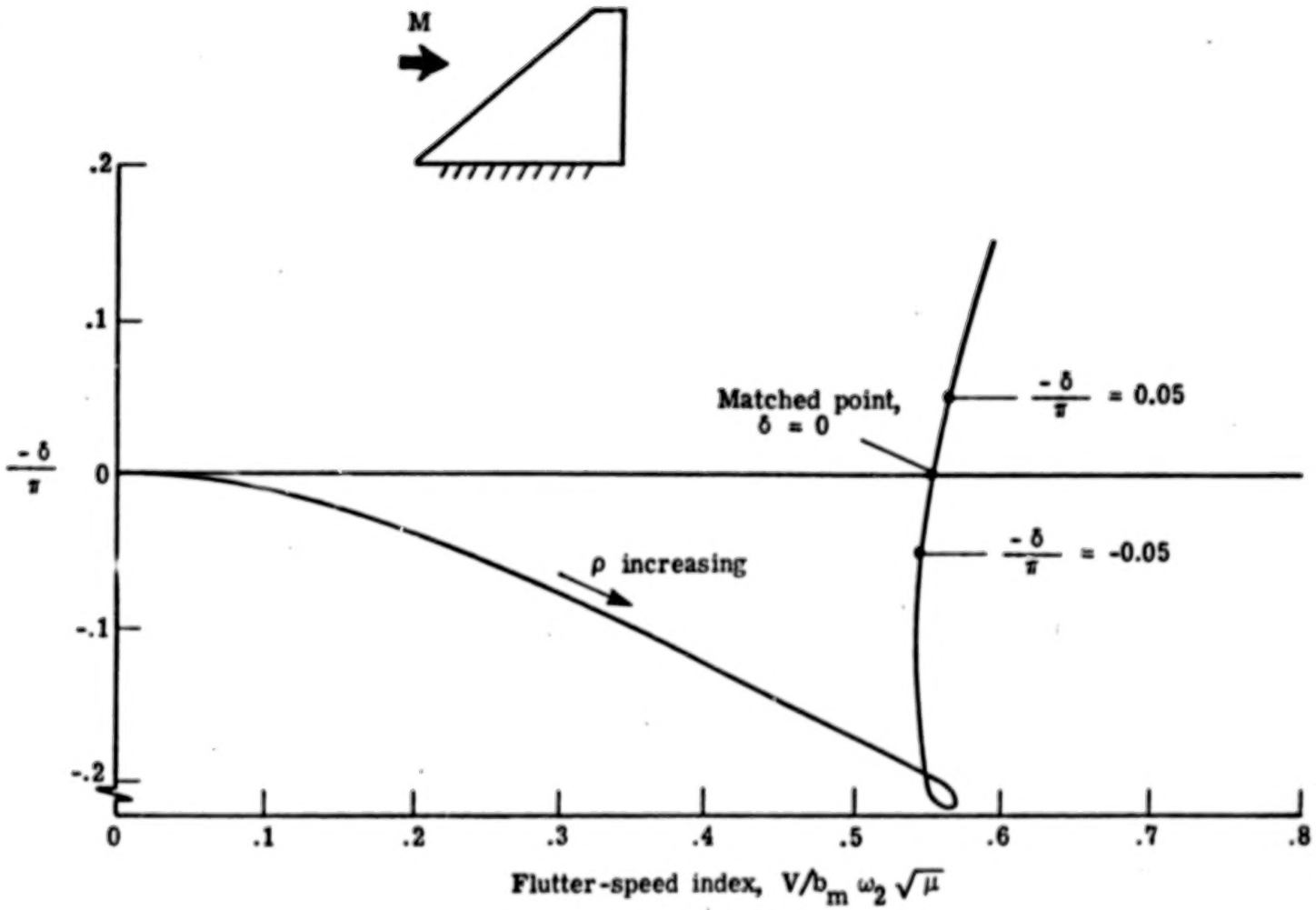
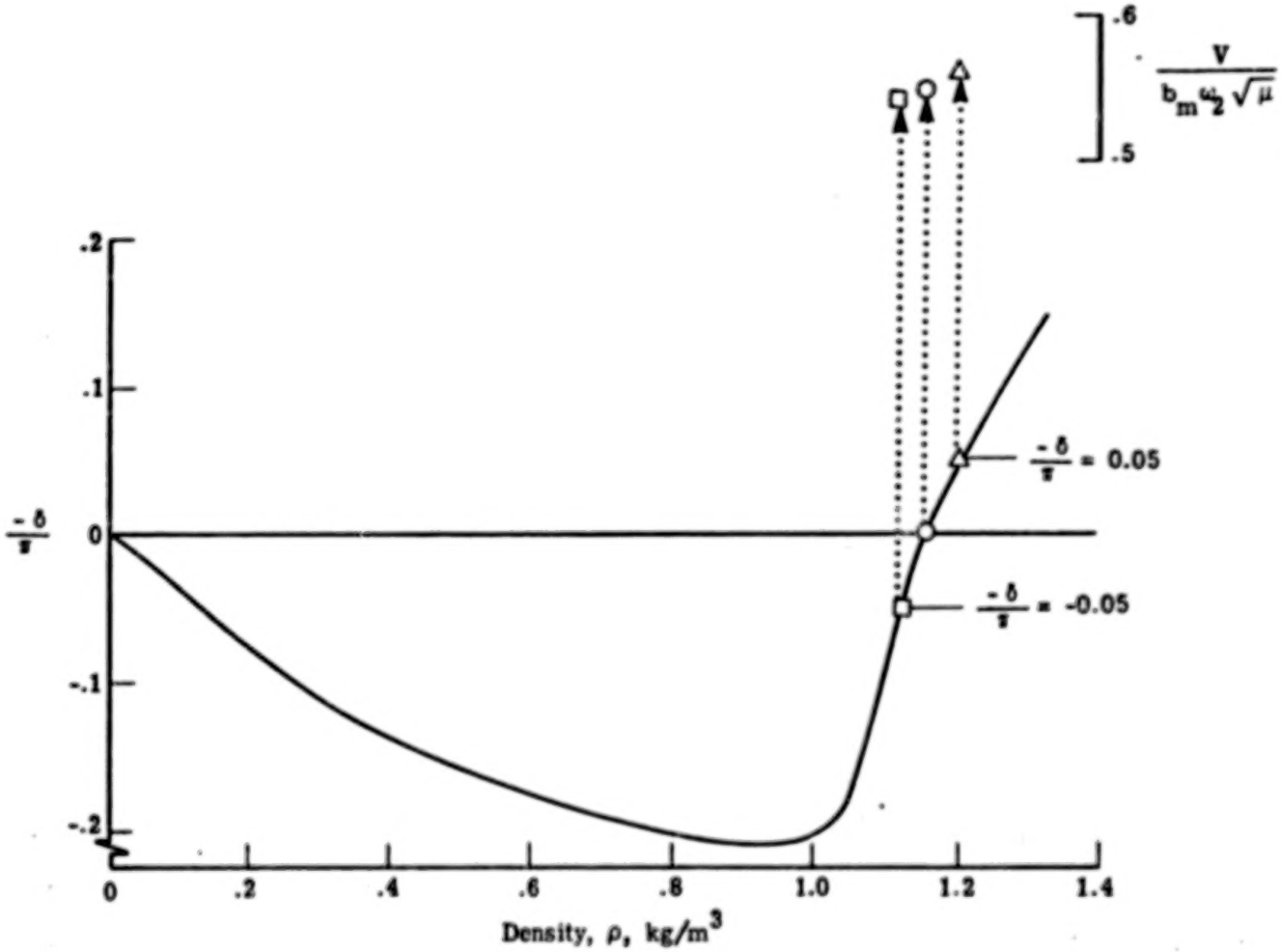


Figure 1.- Lifting surface and coordinate system.



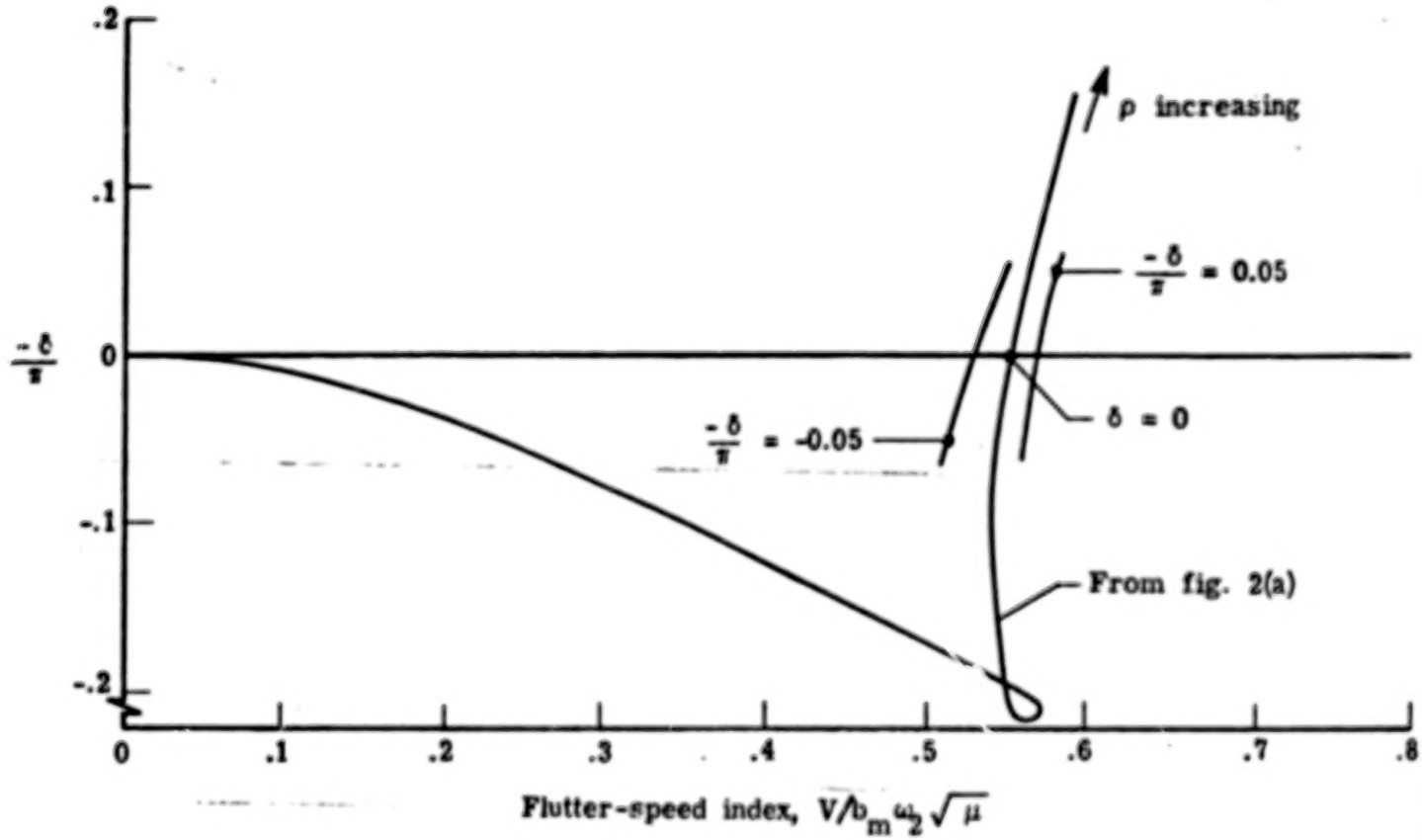
(a) $-\delta/\pi$ plotted against $V/b_m\omega_2\sqrt{\mu}$.

Figure 2.- Flutter and near-flutter eigensolutions obtained with simple harmonic aerodynamics ($\delta = 0$) for clipped delta-wing model of reference 15. $M = 1.3$, $k = 0.47$, and $g_l = 0$. Only critical (mode 2) root is shown.



(b) $-\delta/\pi$ plotted against ρ, and matched point for $\delta = 0$ and intersection points for $-\delta/\pi = \pm 0.05$ in plane of $V/b_m\omega_2\sqrt{\mu}$ plotted against ρ (at upper right).

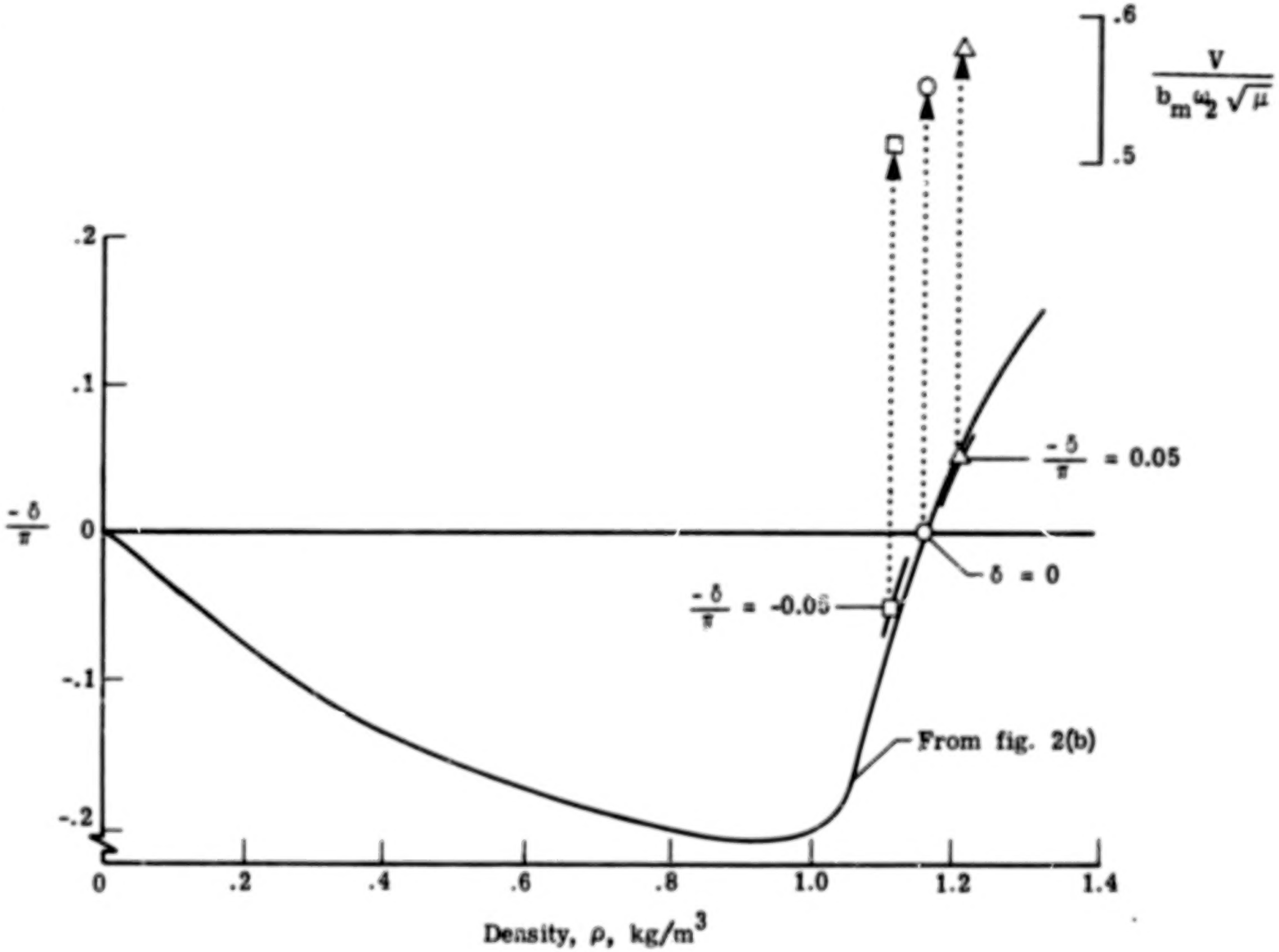
Figure 2.- Concluded.



(a) $-\delta/\pi$ plotted against $V/b_m\omega_2\sqrt{\mu}$.

Figure 3.- Near-flutter eigensolution curve segments obtained with motion-matched aerodynamics, input $-\delta/\pi = \pm 0.05$, for clipped delta-wing model of reference 15, and $\delta = 0$ results from figure 2. $M = 1.3$ and $k = 0.47$. Only critical (mode 2) root is shown.

34



(b) $-\delta/\pi$ plotted against ρ, and matched points of $V/b_m\omega_2\sqrt{\mu}$ plotted against ρ (at upper right).

Figure 3.- Concluded.

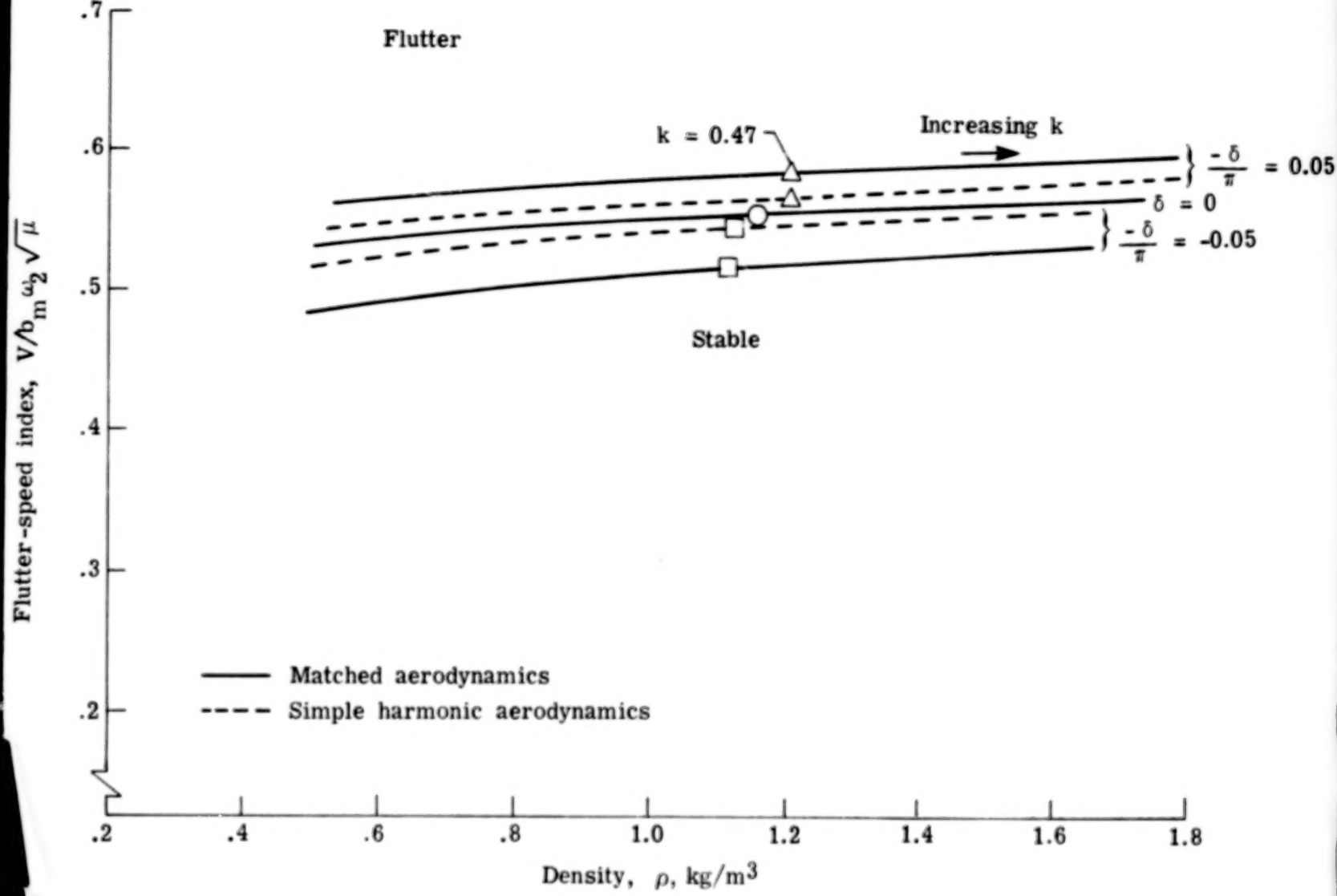


Figure 4.- For clipped delta-wing model, flutter boundary, $\delta = 0$, and isodecrement curves, $-\delta/\pi = \pm 0.05$, in plane of flutter-speed index plotted against density for $M = 1.3$ and range of k-values. Points for $k = 0.47$ from figures 2(b) and 3(b) are indicated.

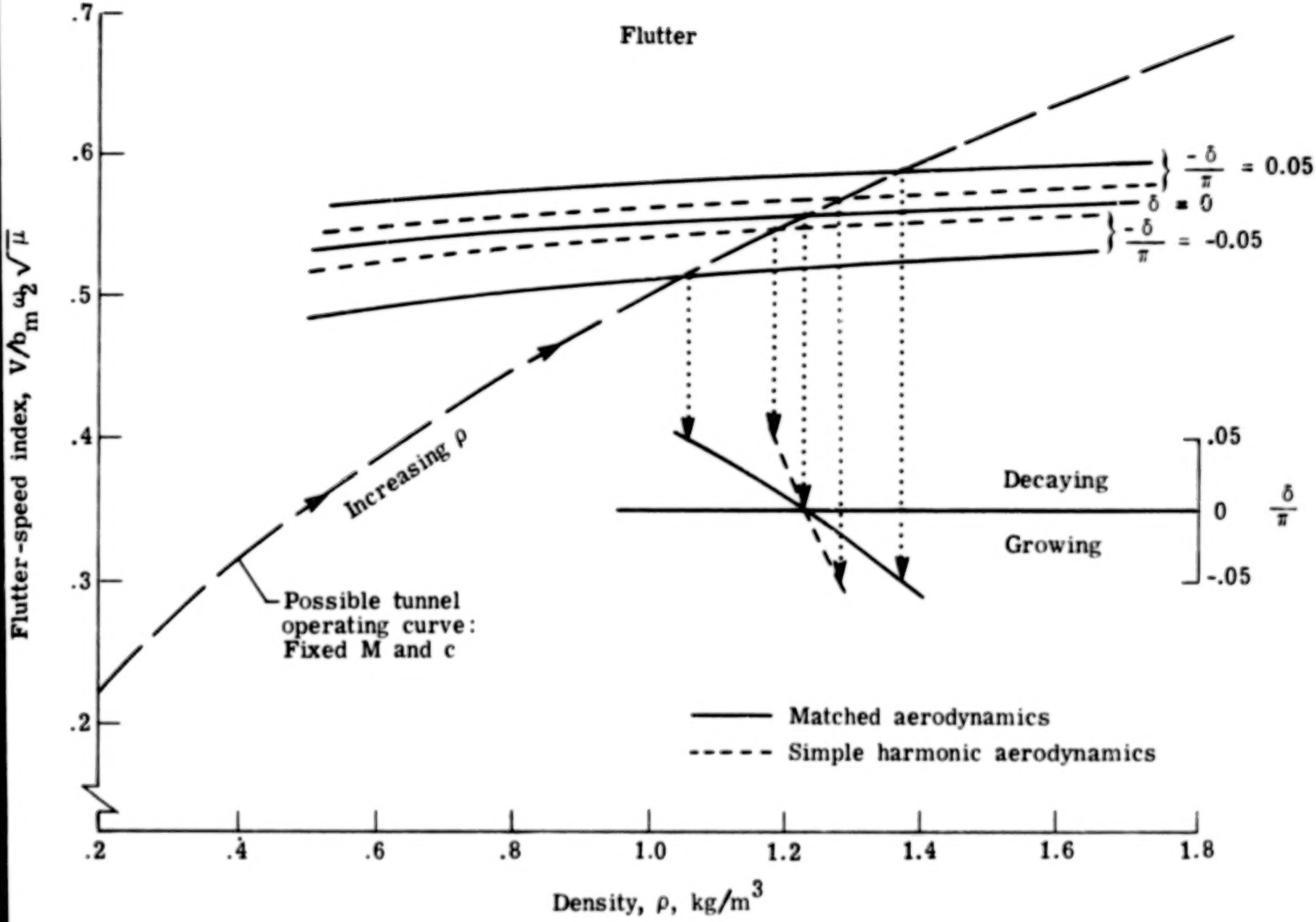


Figure 5.- Possible wind-tunnel operating curve through curves from figure 4, and associated motion decrement plotted as function of density.

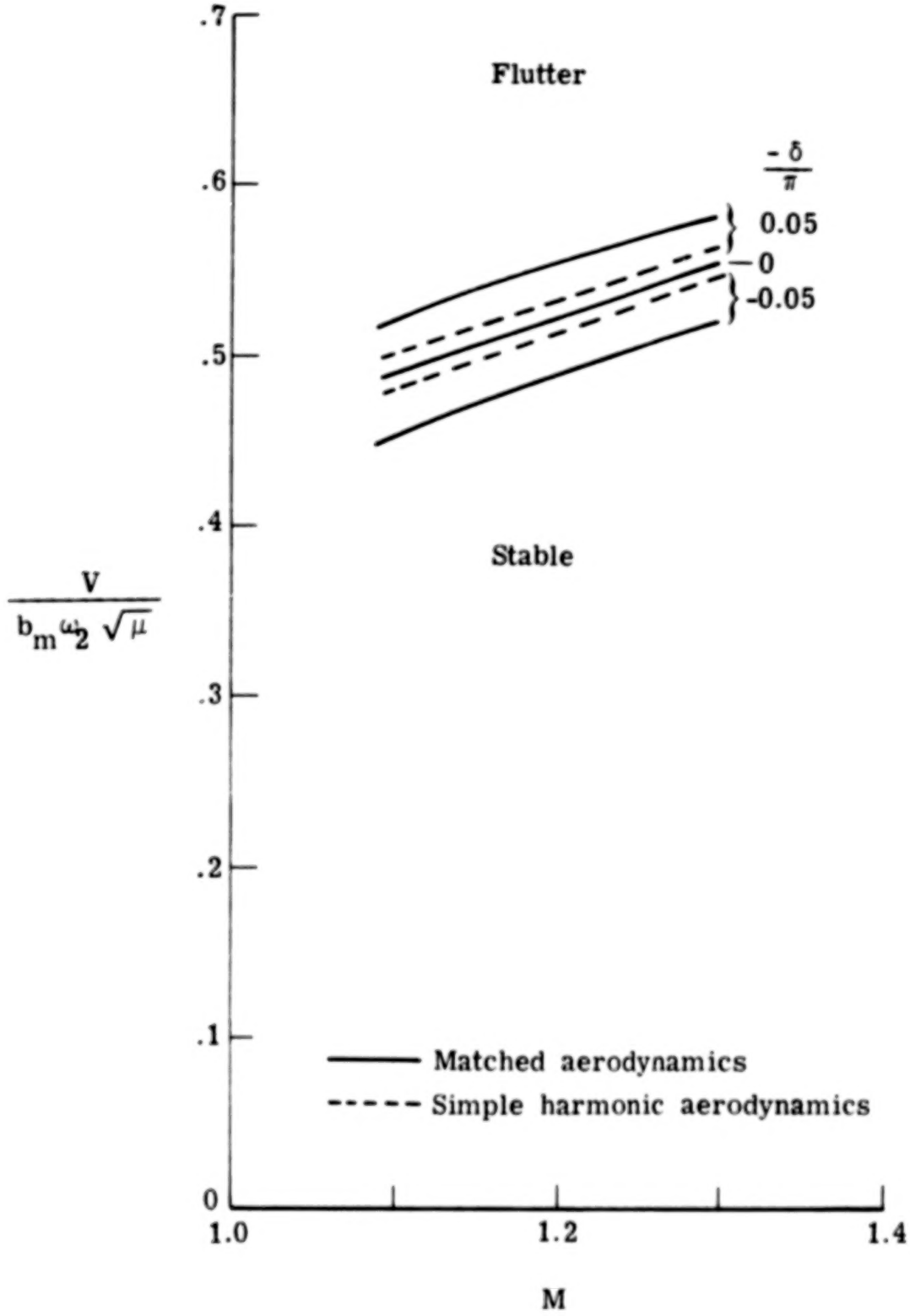
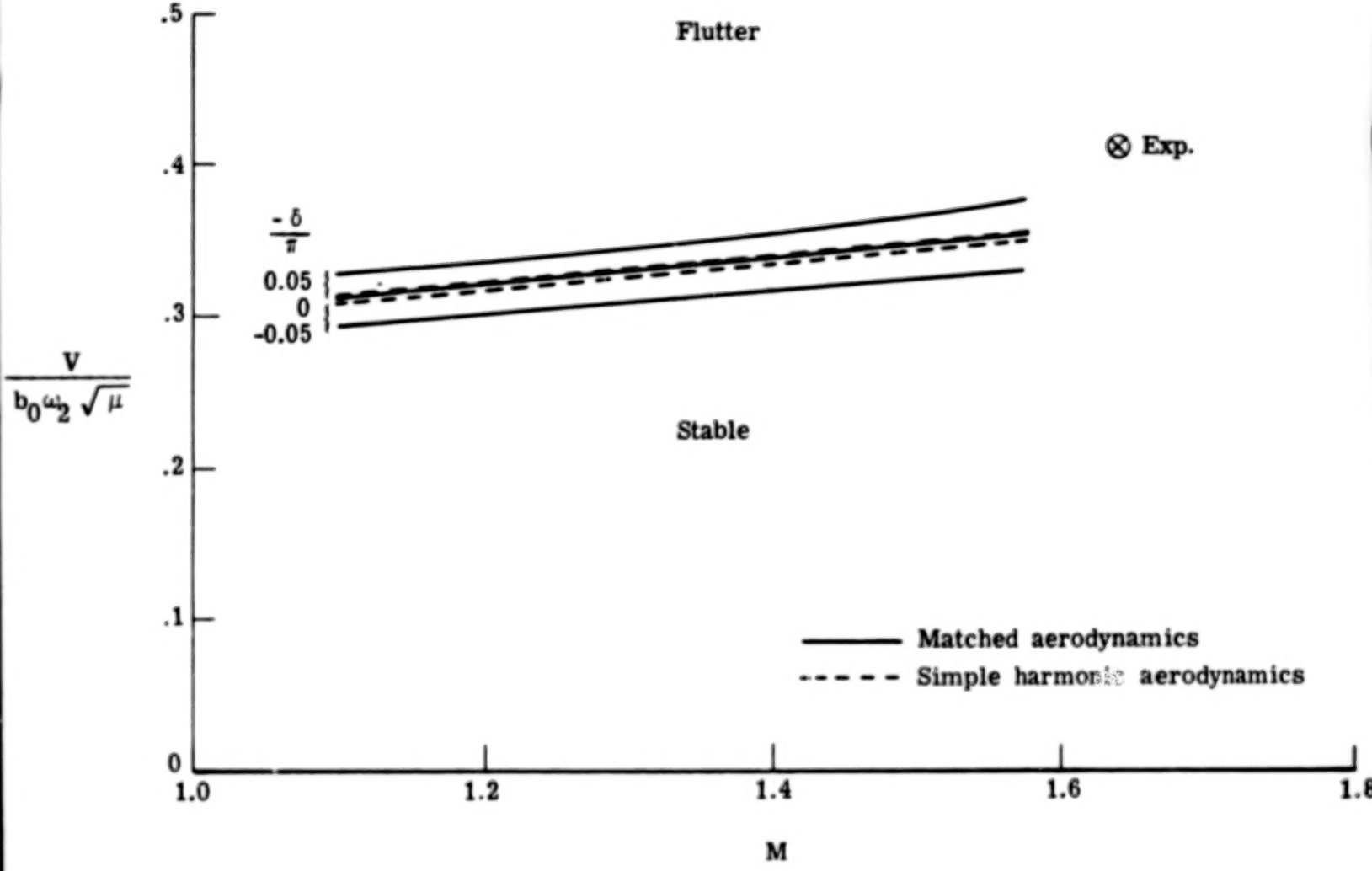
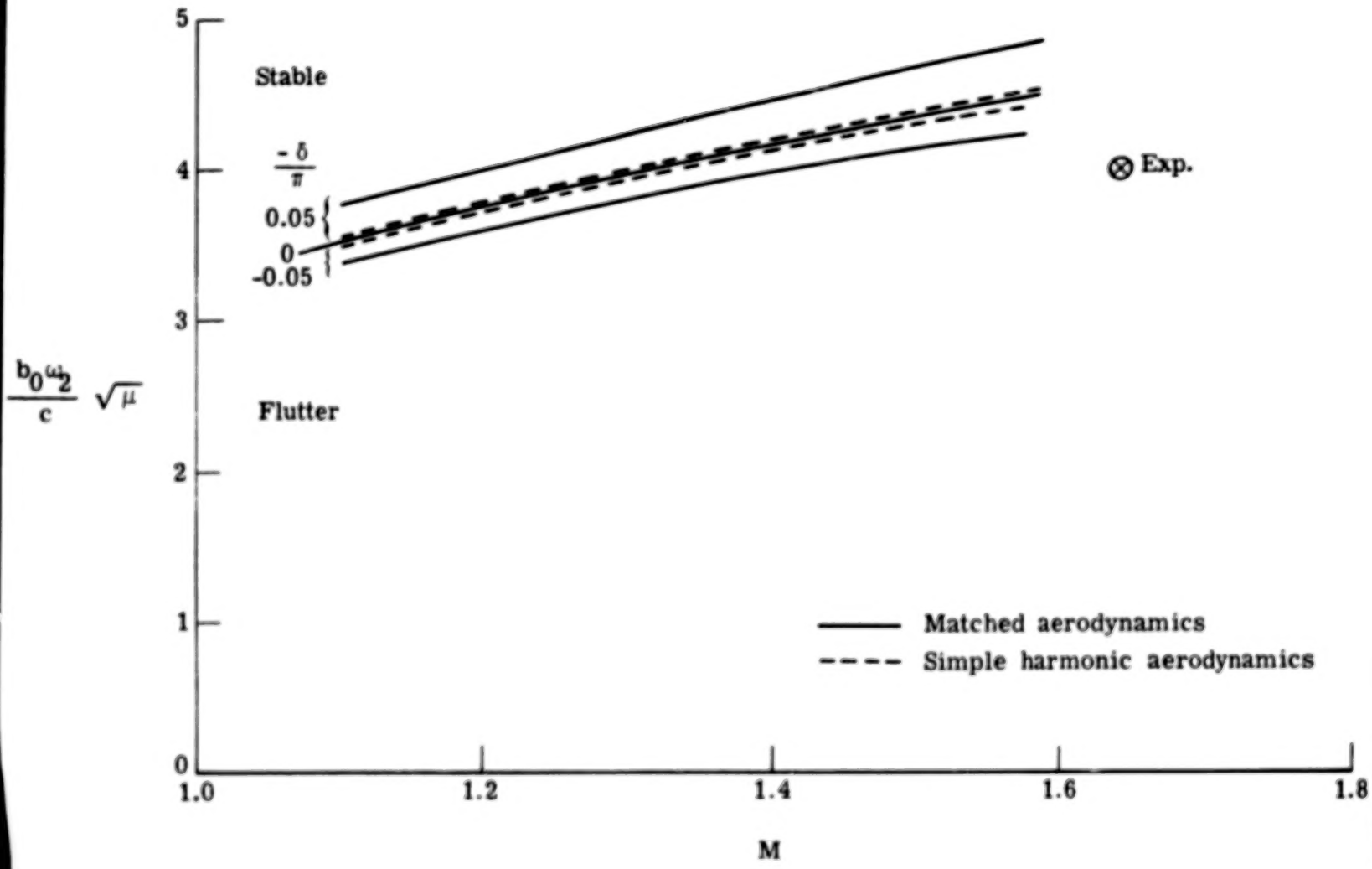


Figure 6.- For clipped delta-wing model, flutter and isodecrement curves in plane of flutter-speed index plotted against M for $\rho = 1.225$ kg/m^3.



(a) Flutter-speed index plotted against M.

Figure 7.- For HT-7 all-movable control model of reference 17 flutter and isodecrement curves for $\rho = 1.70$ kg/m^3.



(b) Stiffness-altitude parameter plotted against M as in reference 17.

Figure 7.- Concluded.

1. Report No. NASA TP-1232	2. Government Accession No.	3. Recipient's Catalog No.
4. Title and Subtitle ANALYSIS OF PREFLUTTER AND POSTFLUTTER CHARACTERISTICS WITH MOTION-MATCHED AERODYNAMIC FORCES		5. Report Date July 1978 6. Performing Organization Code
7. Author(s) Herbert J. Cunningham		8. Performing Organization Report No. L-12109
9. Performing Organization Name and Address NASA Langley Research Center Hampton, VA 23665		10. Work Unit No. 505-02-23-01 11. Contract or Grant No.
12. Sponsoring Agency Name and Address National Aeronautics and Space Administration Washington, DC 20546		13. Type of Report and Period Covered Technical Paper 14. Sponsoring Agency Code

15. Supplementary Notes

16. Abstract

The development of the equations of dynamic equilibrium for a lifting surface from Lagrange's equation is reviewed and restated for general exponential growing and decaying oscillatory motion. Aerodynamic forces for this motion are obtained from the three-dimensional supersonic kernel function that is newly generalized to complex reduced frequencies. Illustrative calculations were made for two flutter models at supersonic Mach numbers. Preflutter and postflutter motion isodecrement curves were obtained. This type of analysis can be used to predict preflutter behavior during flutter testing and to predict postflutter behavior for use in the design of flutter suppression systems.

17. Key Words (Suggested by Author(s))
Flutter analysis
Aeroelasticity
Unsteady aerodynamics
Subcritical flutter
Preflutter
Postflutter

18. Distribution Statement
Unclassified - Unlimited
Subject Category 39

19. Security Classif. (of this report)	20. Security Classif. (of this page)	21. No. of Pages	22. Price*
Unclassified	Unclassified	30	$4.50

* For sale by the National Technical Information Service, Springfield, Virginia 22161

NASA-Langley, 1978